

Research article

Phase Field Theory and Analysis of Pressure-Shear Induced Amorphization and Failure in Boron Carbide Ceramic

John D. Clayton

Impact Physics Branch, US Army Research Laboratory, Aberdeen MD 21005-5066, USA; Email: john.d.clayton1.civ@mail.mil; Tel: +1-410-278-6146; Fax: +1-410-278-2460.

Abstract: A nonlinear continuum phase field theory is developed to describe amorphization of crystalline elastic solids under shear and/or pressure loading. An order parameter describes the local degree of crystallinity. Elastic coefficients can depend on the order parameter, inelastic volume change may accompany the transition from crystal to amorphous phase, and transitional regions parallel to bands of amorphous material are penalized by interfacial surface energy. Analytical and simple numerical solutions are obtained for an idealized isotropic version of the general theory, for an element of material subjected to compressive and/or shear loading. Solutions compare favorably with experimental evidence and atomic simulations of amorphization in boron carbide, demonstrating the tendency for structural collapse and strength loss with increasing shear deformation and superposed pressure.

Keywords: ceramics; phase transformations; amorphization; boron carbide; phase field; elasticity

1. Introduction

Many crystalline ceramics and minerals undergo structural changes (e.g., phase transformations, twinning, or fracture) when subjected to stresses of high magnitude. One such structural transition is amorphization, i.e., transformation from a crystalline structure to an amorphous/glassy phase lacking long-range order. Under mechanical loading by large compressive and/or shear stress, such amorphization may occur, for example, in quartz (α -SiO₂; rhombohedral crystal structure) [1], berlinite (α -AlPO₄; rhombohedral structure) [2], some forms of garnet (Y₃Al₅O₁₂; cubic structure) [3], and boron carbide (nominally B₄C, with varying carbon content possible; rhombohedral) [4]. Noteworthy among all of these materials is a loss of static or dynamic shear stiffness with increasing pressure. According to a theoretical criterion attributed first to Born [5] and advanced in subsequent literature [6-8], attainment of null stiffness in one or more preferred directions, which can be associated with loss of positive-definiteness of a certain tangent elastic stiffness tensor depending on

loading protocol, may signal onset of a localized structural transformation such as amorphization.

The present paper focuses on boron carbide, a strong ceramic of high stiffness, high hardness, low mass density, and low ductility. Different structural variants of boron carbide exist, called polytypes. Atomic chains consisting of C-C-C or C-B-C are aligned parallel to the [0001] direction (hexagonal Miller indices) and thread basal layers of icosahedra at the rhombohedral vertices of the unit cell. Polytypes may differ in stoichiometry, ground state energy, elastic stiffness, and amorphization tendency [9-11]. One model for amorphization based on results of Density Functional Theory (DFT) calculations suggests that structural collapse and localization follow cross-linking of the C-B-C chain with icosahedral atoms [4]; other calculations suggest segregation is most favorable for polytypes with C-C-C chains [9]. More recent DFT calculations [12] demonstrate amorphization in both classes of polytype under uniaxial loading. In physical experiments, amorphization of boron carbide has been observed in Diamond Anvil Cell (DAC) compression-decompression [4], indentation [13], and ballistic impact [14]. Regarding the latter, performance of boron carbide ceramic in protection systems such as armor for vehicles and personnel is thought to be severely impeded by its tendency to localize, with cleavage fracture accompanying or closely following amorphization [14]. In recovered samples, regions of glassy phase are often reported to be in the form of planar bands of small thickness, on the order of several nanometers, and may be preferentially located parallel to certain crystallographic planes [4, 14].

In order to facilitate design of structures and composite material systems for defense and industrial applications, continuum scale models are needed for predicting localization and failure in boron carbide ceramics. Previous models for the transition from crystalline to glassy phase include one based on adiabatic shear localization [15] and another in which instability is triggered by loss of nonlinear elastic tangent stiffness [16, 17] similar to Born's criterion. In contrast, the present paper invokes nonlinear continuum phase field theory, in what appears to be the first known application of phase field modeling towards stress-induced amorphization.

In the phase field approach, the thermodynamic state of the material is described, locally and in part, by one or more order parameters. Elastic strain energy density generally depends on order parameter(s), as does surface energy, the latter reflected by dependence of total energy on spatial gradients of the order parameter(s). Phase field models have been applied to describe numerous kinds of structural changes in crystalline materials, including dislocation glide [18], twinning [19-21], and fracture [22-25]. Advantages of phase field methods over other continuum models for crystal plasticity, twinning, and fracture in metals [26] and ceramics [27-29] include the following: (i) relatively few material parameters are needed, (ii) evolution laws for inelastic deformation mechanisms follow naturally from energy minimization and need not be prescribed ad hoc, and (iii) an intrinsic length scale is introduced via the surface energy, enabling regularization of localization zones and mesh independent numerical results. Regarding the latter advantage, the need for explicit tracking of sharp interfaces is avoided in numerical schemes, and standard finite element discretizations may be used for solution of boundary value problems.

In the present paper, phase field theory is applied towards amorphization in a way similar to prior phase field models for fracture [22-25], with a single order parameter increasing in value from zero to unity during the transition from crystalline to amorphous phase, and with shear stiffness degrading with increasing order parameter. It is clarified that whereas amorphization can be classified as a true phase transformation, twinning and fracture are not usually categorized as such in a strict sense. Regardless, phase field models tend to treat twinning and fracture analogously to phase

changes, wherein evolution of order parameter(s) quantify the transition in state from a perfect parent crystal “phase” to a fully twinned or fully fractured/damaged “phase”. Structural collapse may be accompanied by an inelastic decrease in volume (i.e., increase in mass density) [4], which promotes amorphization with increasing pressure. Thus, under pressure, shear stiffness and strength tend to decrease, in agreement with DFT calculations [10-12]. In the present paper, a general thermodynamic theory is developed first, accounting for anisotropic elastic strain energy and anisotropic surface energy. Then an idealized nonlinear isotropic theory is developed that facilitates solution of boundary value problems. Specifically, problems involving volumetric compression and simple shear and are studied analytically to demonstrate the predictive ability of the theory. Stability is assessed, extending previous analyses of continuum damage models [30]. Effects of properties particular and peculiar to boron carbide entering the model are explored, providing new insight into the onset of localization and failure. Notation of nonlinear continuum mechanics [31] is used, here primarily in direct form for vectors and tensors which are written in bold font.

2. Materials and Method

2.1. Boron Carbide

Single crystals of boron carbide (B_4C) belong to space group $R\bar{3}m$, centrosymmetric point group $\bar{3}m$, and Laue group RI, the latter indicative of six independent second-order elastic constants and fourteen independent third-order elastic constants [16, 31]. The theoretical mass density of stoichiometric B_4C is $2.52 \text{ g}\cdot\text{cm}^{-3}$. Polycrystalline boron carbide has a typical grain size on the order of $10 \text{ }\mu\text{m}$, an elastic modulus on the order of 470 GPa , a hardness on the order of 30 GPa , and a Hugoniot Elastic Limit (HEL, or yield stress under shock compression) on the order of $15\text{-}20 \text{ GPa}$ [17]. Ductility is low, implying that although full dislocations, partial dislocations, and stacking faults have been observed [32], their low-temperature mobility is inhibited [16]. Twins are thought to arise predominantly during processing [33] rather than to be induced by stress or strain. Primary inelastic deformation mechanisms under impact loading are amorphization and fracture (primarily cleavage fracture on intrinsically weakest planes), which may occur sequentially or simultaneously.

Table 1. Properties of boron carbide.

Property	Description	Value [units]
B_0	bulk modulus (crystal)	248 GPa
μ_0	shear modulus (crystal)	197 GPa
l	localization width (glass)	2 nm
Γ	surface energy (glass)	$347 \text{ mJ}\cdot\text{m}^{-2}$
Ξ	density ratio (crystal/glass)	0.96

Listed for future reference in Table 1 are physical properties entering the idealized isotropic phase field model of boron carbide to be applied later in analysis of pressure-shear deformation and corresponding instability. Ambient bulk modulus B_0 and shear modulus μ_0 for the fully crystalline phase are obtained, respectively, from a fit of the nonlinear elastic potential function to quantum mechanical equation-of-state data for the polar C-B-C polytype [11] and a Voigt average of the second-order anisotropic constants [29, 31]. Regularization parameter l indicating the width of

localized structural transition zones is representative of the thickness of planar glassy phases of boron carbide observed in recovered experimental samples [4, 14]. The surface energy of amorphous zones is computed as the difference between ground state energies (measured per appropriate unit reference volume) of segregated amorphous and crystal phases, multiplied by l , where energy of the polar C-B-C polytype is used for the crystal reference [9]. The ratio of mass density of the crystalline phase to that of the amorphous phase is denoted by Ξ ; this value depends on the composition and structure of the glass, here taken as 0.96, corresponding to a 4% volume reduction upon structure collapse commensurate with amorphization [4].

2.2. Phase Field Theory: General

General nonlinear, anisotropic, three-dimensional (3D) theory is outlined in §2.2. Model kinematics, energy functions, and governing equations are described in turn.

2.2.1. Kinematics

Let $\mathbf{x} = \mathbf{x}(\mathbf{X}, t)$ denote spatial position at time t of a material particle whose reference position is denoted by \mathbf{X} . The deformation gradient is

$$\mathbf{F} = \nabla \mathbf{x} = \partial \mathbf{x} / \partial \mathbf{X} \quad (1)$$

where ∇ is the material gradient operator. Let $\xi \in [0, 1]$ denote the scalar order parameter, where

$$\xi(\mathbf{X}, t) \begin{cases} = 0 & \forall \mathbf{X} \in \text{crystal phase at time } t \\ \in (0, 1) & \forall \mathbf{X} \in \text{interface zone at time } t \\ = 1 & \forall \mathbf{X} \in \text{glassy phase at time } t \end{cases} \quad (2)$$

The deformation gradient is split multiplicatively into a product of two terms as

$$\mathbf{F} = \mathbf{F}^E \mathbf{F}^\xi, \quad \mathbf{F}^\xi(\mathbf{X}, t) = \mathbf{F}^\xi[\xi(\mathbf{X}, t)] \quad (3)$$

where \mathbf{F}^E is the elastic deformation conjugate to the applied stress and \mathbf{F}^ξ is the inelastic deformation that depends, as indicated, on the local value of the order parameter associated with structural transformation, specifically amorphization. Unlike \mathbf{F} , which always obeys compatibility (null curl) conditions $\nabla \times \mathbf{F} = 0$, neither \mathbf{F}^E nor \mathbf{F}^ξ is individually always integrable to a vector field, i.e., these two deformations are generally anholonomic [34]. Note that this theory only accounts explicitly for one type of structural change. Not included in (3) are additional terms needed for representation of effects of other kinds of defects, for example dislocation slip [26, 31], twinning [27], fracture [35], disclination rotation [36], and dilatation associated with stacking faults and dislocation or disclination cores [37, 38] or point defects [39, 40]. The symmetric elastic deformation tensor \mathbf{C} and the measure of elastic volume change J are defined as (no “E” superscript)

$$\mathbf{C} = (\mathbf{F}^E)^T \mathbf{F}^E, \quad J = \sqrt{\det \mathbf{C}} = \det \mathbf{F}^E = \det \mathbf{F} / \det \mathbf{F}^\xi \quad (4)$$

2.2.2. Energy Functional

Similar to previous nonlinear phase field theories for twinning [19-21] and fracture [25], a total energy functional for a body of reference volume V is posited in general form as

$$\Psi(\mathbf{x}, \xi) = \int_V [W(\mathbf{C}, \xi) + f(\xi) + \boldsymbol{\kappa} : \nabla \xi \otimes \nabla \xi] dV \quad (5)$$

where W is elastic strain energy density per unit reference volume, f accounts for the difference in ground state energies among crystalline, amorphous, and intermediate phases, and $\boldsymbol{\kappa}$ is a symmetric second-order tensor that accounts for surface energy associated with gradients of the order parameter. For a fully realistic nonlinear anisotropic response, W should reflect the rhombohedral symmetry of the crystalline phase, the importance of higher-order elastic constants [16], and the transition to elastic isotropy upon complete amorphization [17]. In order to restrict amorphous bands to specific crystallographic planes, the following form of $\boldsymbol{\kappa}$ may be used [25]:

$$\boldsymbol{\kappa} = \kappa_0 [\mathbf{1} + \beta(\mathbf{1} - \mathbf{m} \otimes \mathbf{m})] \quad (6)$$

Here κ_0 is a scalar and $\beta \geq 0$ is a penalty factor that, when greater than zero, increases surface energies on planes not normal to referential unit vector \mathbf{m} . If such a representation is insufficient (i.e., if numerous different planes with various surface energies and orientations are prone to localization), the theory may require extension to distinct order parameters for each plane.

2.2.3. Governing Equations

A variational framework is considered henceforth, amenable to solution via energy minimization [19-21]. Time t becomes a parameter and does not explicitly enter the governing equations, which are now applicable only to quasi-static problems. The following variational principle is set forth:

$$\delta\Psi = \iint_S [\mathbf{t} \cdot \delta\mathbf{x} + r\delta\xi] dS \quad (7)$$

with \mathbf{t} the mechanical traction vector, r a conjugate force to the order parameter, and S the referential surface enclosing V . Application of standard mathematical procedures involving integration by parts and the divergence theorem [19, 31] results in the following local equilibrium equations (i.e., Euler-Lagrange equations) in V and natural boundary conditions on S :

$$\nabla \cdot \mathbf{P} = 0, \quad \mathbf{P} = (\partial W / \partial \mathbf{F})|_{\xi} \quad (8)$$

$$\varsigma + df/d\xi = 2\boldsymbol{\kappa} \nabla^2 \xi, \quad \varsigma = (\partial W / \partial \xi)|_F \quad (9)$$

$$\mathbf{t} = \mathbf{P} \cdot \mathbf{n}, \quad r = 2\boldsymbol{\kappa} : \nabla \xi \otimes \mathbf{n} \quad (10)$$

The first Piola-Kirchhoff stress tensor is \mathbf{P} , and the unit outward normal vector to S is \mathbf{n} .

2.3. Phase Field Theory: Idealized

The nonlinear theory of §2.2 is now specialized to isotropic behavior. This model, which is far more amenable to analytical and simple numerical solutions than that of §2.2, can be applied to gain insight into particular problems (e.g., 1D) wherein anisotropy is of secondary importance. Model kinematics, energy functions, and governing equations are again described in turn.

2.3.1. Kinematics

Equations (1)-(4) still apply. Inelastic deformation corresponding to amorphization is specified as the isotropic volume change (i.e., spherical eigenstrain)

$$\mathbf{F}^\xi(\xi) = [\phi(\xi)]^{1/3} \mathbf{1}; \quad \phi(0) = 1, \quad \phi(1) = \Xi \quad (11)$$

with ϕ a sufficiently smooth, positive scalar function of the order parameter and with Ξ introduced in §2.1. A similar construction has been used elsewhere to model residual volume changes from point defects [40] and pore collapse [41]. Equation (4) then reduces to

$$\mathbf{C}(\mathbf{F}, \xi) = [\phi(\xi)]^{-2/3} \mathbf{F}^T \mathbf{F}, \quad J(\mathbf{F}, \xi) = \det \mathbf{F} / \phi(\xi) \quad (12)$$

2.3.2. Energy Functional

Equations (5) and (6) still apply. A compressible neo-Hookean nonlinear elastic strain energy potential [20, 21, 25] is prescribed:

$$W(\mathbf{C}, \xi) = \frac{1}{2} \mu (\text{tr} \mathbf{C} - 3 - 2 \ln J) + \frac{1}{2} \lambda (\ln J)^2 \quad (13)$$

Elastic coefficients may depend on the order parameter ξ :

$$\mu = \mu_0 \chi(\xi), \quad \lambda = \lambda_0 \mathfrak{t}(\xi); \quad \lambda_0 = B_0 - \frac{2}{3} \mu_0, \quad \chi(0) = \mathfrak{t}(0) = 1 \quad (14)$$

Here, χ and \mathfrak{t} are sufficiently smooth scalar functions of the order parameter that interpolate between elastic constants of crystal and glass phases. Isotropic bulk and surface energies of the amorphous phase are represented by

$$f(\xi) = \Gamma \xi^2 / l, \quad \boldsymbol{\kappa} : \nabla \xi \otimes \nabla \xi = \Gamma l |\nabla \xi|^2 \quad (\kappa_0 = \Gamma l, \beta = 0) \quad (15)$$

where surface energy per unit reference area Γ and regularization length l have been introduced in §2.1. Total energy (5) then becomes

$$\Psi(\mathbf{x}, \xi) = \int_V [W(\nabla \mathbf{x}, \xi) + \Gamma \xi^2 / l + \Gamma l |\nabla \xi|^2] dV \quad (16)$$

with strain energy (13) expressed explicitly in terms of ξ and $\mathbf{F} = \nabla \mathbf{x}$ as

$$W(\mathbf{F}, \xi) = \frac{1}{2} \mu_0 \chi(\xi) \{ [\phi(\xi)]^{-2/3} \mathbf{F} : \mathbf{F} - 3 - 2 \ln [\det \mathbf{F} / \phi(\xi)] \} + \frac{1}{2} \lambda_0 \mathfrak{t}(\xi) \{ \ln [\det \mathbf{F} / \phi(\xi)] \}^2 \quad (17)$$

As a point of clarification, the term “interpolation function” is used herein to refer to any of functions ϕ , χ , and \mathfrak{t} that depend continuously on values of order parameter ξ . These functions are used to estimate values of specific volume and elastic coefficients in material wherein transformation is incomplete (i.e., wherein $0 < \xi < 1$), given, a priori, known values of such quantities at the endpoints $\xi = 0$ and $\xi = 1$ corresponding to pure crystalline and amorphous phases, respectively.

2.3.3. Governing Equations

Equations (7)-(10) still apply. Using (13), stress in the second of (8) and elastic driving force in the second of (9) become, respectively,

$$\mathbf{P}(\mathbf{F}, \xi) = \mu_0 \chi(\xi) \{ [\phi(\xi)]^{-2/3} \mathbf{F} - \mathbf{F}^{-T} \} + \lambda_0 \mathfrak{u}(\xi) \ln[\det \mathbf{F} / \phi(\xi)] \mathbf{F}^{-T} \quad (18)$$

$$\begin{aligned} \varsigma(\mathbf{F}, \xi) = & \phi'(\xi) \{ \mu_0 \chi(\xi) / \phi(\xi) - \frac{1}{3} \mu_0 \chi(\xi) [\phi(\xi)]^{-5/3} \mathbf{F} : \mathbf{F} - \lambda_0 [\mathfrak{u}(\xi) / \phi(\xi)] \ln[\det \mathbf{F} / \phi(\xi)] \} \\ & + \chi'(\xi) \mu_0 \{ \frac{1}{2} [\phi(\xi)]^{-2/3} \mathbf{F} : \mathbf{F} - \frac{3}{2} - \ln[\det \mathbf{F} / \phi(\xi)] \} + \frac{1}{2} \mathfrak{u}'(\xi) \lambda_0 \{ \ln[\det \mathbf{F} / \phi(\xi)] \}^2 \end{aligned} \quad (19)$$

where $\phi' = d\phi/d\xi$, $\chi' = d\chi/d\xi$, and $\mathfrak{u}' = d\mathfrak{u}/d\xi$. Cauchy stress tensor $\boldsymbol{\sigma} = (1/\det \mathbf{F}) \mathbf{P} \mathbf{F}^T$ and Cauchy pressure $p = -\text{tr} \boldsymbol{\sigma} / 3$ are, respectively,

$$\boldsymbol{\sigma}(\mathbf{F}, \xi) = [\mu_0 \chi(\xi) / \det \mathbf{F}] \{ [\phi(\xi)]^{-2/3} \mathbf{F} \mathbf{F}^T - \mathbf{1} \} + [\lambda_0 \mathfrak{u}(\xi) / \det \mathbf{F}] \ln[\det \mathbf{F} / \phi(\xi)] \mathbf{1} \quad (20)$$

$$p(\mathbf{F}, \xi) = [\mu_0 \chi(\xi) / \det \mathbf{F}] \{ 1 - \frac{1}{3} [\phi(\xi)]^{-2/3} \mathbf{F} : \mathbf{F} \} - [\lambda_0 \mathfrak{u}(\xi) / \det \mathbf{F}] \ln[\det \mathbf{F} / \phi(\xi)] \quad (21)$$

3. Results

Analyzed are solutions of the phase field theory of §2.3 for spatially homogeneous hydrostatic compression, followed by solutions for combined spherical compression and simple shear.

3.1. Hydrostatic Compression

First consider uniform spherical deformation of an element of initially fully crystalline material from reference/initial volume V to current volume v :

$$\mathbf{x} = A^{1/3} \mathbf{X}; \quad \mathbf{F} = A^{1/3} \mathbf{1}; \quad A = \det \mathbf{F} = v/V > 0 \quad (\nabla A = 0) \quad (22)$$

Under such spherical deformation, (18)-(21) reduce to

$$\mathbf{P}(A, \xi) = \mu_0 \chi(\xi) \{ [\phi(\xi)]^{-2/3} A^{1/3} - A^{-1/3} \} \mathbf{1} + \lambda_0 \mathfrak{u}(\xi) A^{-1/3} \ln[A/\phi(\xi)] \mathbf{1} \quad (23)$$

$$\begin{aligned} \varsigma(A, \xi) = & \phi'(\xi) \{ \mu_0 \chi(\xi) / \phi(\xi) - \mu_0 \chi(\xi) [\phi(\xi)]^{-5/3} A^{2/3} - \lambda_0 [\mathfrak{u}(\xi) / \phi(\xi)] \ln[A/\phi(\xi)] \} \\ & + \chi'(\xi) \mu_0 \{ \frac{3}{2} [\phi(\xi)]^{-2/3} A^{2/3} - \frac{3}{2} - \ln[A/\phi(\xi)] \} + \frac{1}{2} \mathfrak{u}'(\xi) \lambda_0 \{ \ln[A/\phi(\xi)] \}^2 \end{aligned} \quad (24)$$

$$\boldsymbol{\sigma}(A, \xi) = [\mu_0 \chi(\xi) / A] \{ [\phi(\xi)]^{-2/3} A^{2/3} - 1 \} \mathbf{1} + [\lambda_0 \mathfrak{u}(\xi) / A] \ln[A/\phi(\xi)] \mathbf{1} \quad (25)$$

$$p(A, \xi) = [\mu_0 \chi(\xi) / A] \{ 1 - [A/\phi(\xi)]^{2/3} \} - [\lambda_0 \mathfrak{u}(\xi) / A] \ln[A/\phi(\xi)] \quad (26)$$

In Cartesian coordinates $\mathbf{x} = (x, y, z)$ and $\mathbf{X} = (X, Y, Z)$, stress equilibrium in the first of (8) with (22) and (23) reduces to

$$\partial P_{xx} / \partial X = \partial P_{yy} / \partial Y = \partial P_{zz} / \partial Z = 0 \Rightarrow P = P_{xx} = P_{yy} = P_{zz} = \text{constant} \quad (27)$$

$$\nabla P(A, \xi) = (\partial P / \partial A) \nabla A + (\partial P / \partial \xi) \nabla \xi = 0 \Rightarrow \xi = \text{constant} \quad (28)$$

Order parameter equilibrium in the first of (9) with equations (15), (24), and (28) becomes the algebraic equation

$$\xi = -\frac{1}{2}(l/\Gamma)\phi'[\mu_0\chi/\phi - \mu_0\chi\phi^{-5/3}A^{2/3} - \lambda_0(\iota/\phi)\ln(A/\phi)] - \frac{1}{2}(l/\Gamma)\chi'\mu_0[\frac{3}{2}\phi^{-2/3}A^{2/3} - \frac{3}{2} - \ln(A/\phi)] - \frac{1}{4}(l/\Gamma)\iota'\lambda_0[\ln(A/\phi)]^2 \quad (29)$$

Solution of this equation requires specification of interpolation functions $\phi(\xi)$, $\chi(\xi)$, and $\iota(\xi)$. Similar to the polynomial form used elsewhere in a phase field model for twinning [19-21], let

$$\phi = \Xi + (1 - \Xi)[3(1 - \xi)^2 - 2(1 - \xi)^3], \quad \phi' = -6(1 - \Xi)[(1 - \xi) - (1 - \xi)^2] \quad (30)$$

Similar to phase field models for fracture invoked elsewhere [22-25], the shear modulus degrades as

$$\chi = (1 - \xi)^2, \quad \chi' = -2(1 - \xi) \quad (31)$$

This is consistent with the reported loss of shear strength in localized amorphous bands in boron carbide [4, 14, 16]. Transformation can also be interpreted to correlate with mode II fracture in this model. Now let the ambient bulk modulus B_0 remain constant upon amorphization, which requires from (31) that

$$\iota = B_0/\lambda_0 - \frac{2}{3}(1 - \xi)^2\mu_0/\lambda_0 = \frac{1}{3}[1 + \nu_0 - (1 - \xi)^2(1 - 2\nu_0)]/\nu_0$$

$$\iota' = \frac{2}{3}(1 - \xi)(1 - 2\nu_0)/\nu_0 \quad (32)$$

with ν_0 Poisson's ratio for the crystalline phase. Prior DFT calculations [42] have suggested a $\approx 4\%$ decrease in bulk modulus may occur upon structure transformation; this change is considered small enough, and of the same order of accuracy as the DFT solutions, to be justifiably ignored, thereby simplifying the theoretical framework and analytical solutions.

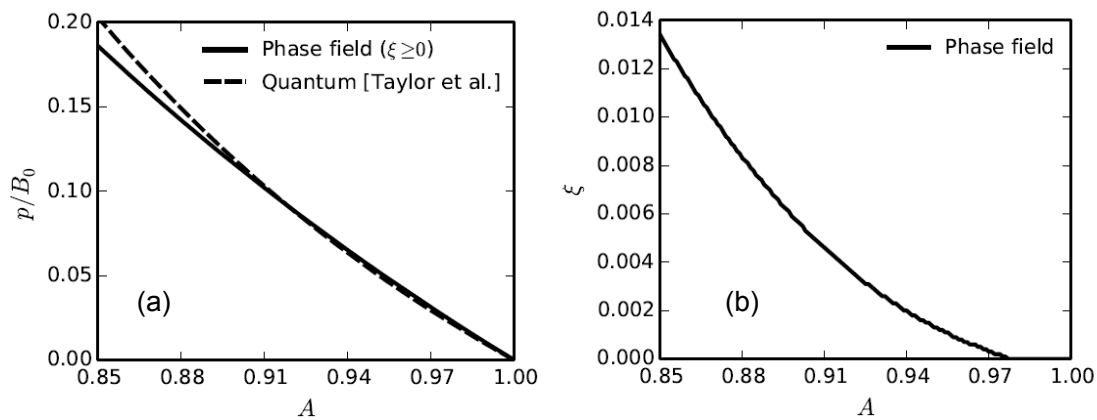


Figure 1. Pressure-volume response (a) and order parameter evolution (b) under uniform spherical compression.

Solution data are obtained as follows for hydrostatic compressive loading. Volume is reduced incrementally by decreasing A from an initial condition of unity. For each volume decrement, (29) is solved via simple numerical iteration to obtain order parameter ξ . Once ξ is known, functions (30)-(32) are evaluated and then substituted into analytical expression (26) to determine pressure p . Compared in Figure 1(a) are the pressure predicted from the present phase field model and results of quantum (DFT) calculations [11] for the polar C-B-C polytype, which were fit to a Birch-Murnaghan equation-of-state [43]. Agreement between the two sets of results is deemed excellent for $A \geq 0.9$, i.e., for volumetric compression less than around 10%. As shown in Figure 1(b), ξ remains very small for

compressions up to 15%; in fact, the phase field model predicts $\xi < 0.1$ for $A > 0.64$. Such predictions agree with DFT simulations that do not indicate transformation or amorphization occurs in boron carbide for purely hydrostatic loading [11, 12]. A measure of intrinsic stability [6-8] under hydrostatic loading requires that the slope of the pressure-volume curve remains negative:

$$-dp dv = -dp d(AV) = -V(\partial p/\partial A)(dA)^2 > 0 \Rightarrow \partial p/\partial A < 0 \quad (33)$$

This stability condition, which correlates with a positive incremental/tangent bulk modulus, is clearly satisfied by the solutions in Figure 1(a), demonstrating mechanical stability of boron carbide under purely hydrostatic compression to large pressures.

3.2. Simple Shear under Constant Compression

Now consider spherical deformation of an element of initially fully crystalline material of length L superposed with shear displacement of magnitude v that potentially varies only with the X coordinate. In Cartesian coordinates, the deformation, deformation gradient matrix, Jacobian determinant, and shear strain are, respectively,

$$\begin{aligned} x &= A^{1/3} X \\ y &= A^{1/3} Y + v(X), \\ z &= A^{1/3} Z \end{aligned} \quad \mathbf{F} = \begin{bmatrix} A^{1/3} & 0 & 0 \\ \gamma & A^{1/3} & 0 \\ 0 & 0 & A^{1/3} \end{bmatrix}, \quad A = \det \mathbf{F} > 0, \quad \gamma = dv/dX \quad (34)$$

Here, A is constant with respect to reference coordinates ($\nabla A = 0$), but γ may generally vary with X , where $X \in [0, L]$. Under such shearing and volumetric deformation, (18), (19), and (21) reduce to

$$\begin{aligned} P_{xx}(A, \xi) &= P_{yy}(A, \xi) = P_{zz}(A, \xi) \\ &= \mu_0 \chi(\xi) A^{-1/3} \{[\phi(\xi)]^{-2/3} A^{2/3} - 1\} + \lambda_0 v(\xi) A^{-1/3} \ln[A/\phi(\xi)] \\ P_{xy}(A, \gamma, \xi) &= \{\mu_0 \chi(\xi) - \lambda_0 v(\xi) \ln[A/\phi(\xi)]\} \gamma \end{aligned} \quad (35)$$

$$P_{yx}(A, \gamma, \xi) = \{\mu_0 \chi(\xi) [\phi(\xi)]^{-2/3}\} \gamma = \tau$$

$$P_{xz} = P_{yz} = P_{zx} = P_{zy} = 0$$

$$\begin{aligned} \varsigma(A, \gamma, \xi) &= \phi'(\xi) \{ \mu_0 \chi(\xi) / \phi(\xi) - \mu_0 \chi(\xi) [\phi(\xi)]^{-5/3} A^{2/3} - \lambda_0 [v(\xi) / \phi(\xi)] \ln[A/\phi(\xi)] \} \\ &+ \chi'(\xi) \mu_0 \{ \frac{3}{2} [\phi(\xi)]^{-2/3} A^{2/3} - \frac{3}{2} - \ln[A/\phi(\xi)] + \frac{1}{2} \gamma^2 \} + \frac{1}{2} v'(\xi) \lambda_0 \{ \ln[A/\phi(\xi)] \}^2 \end{aligned} \quad (36)$$

$$p(A, \gamma, \xi) = [\mu_0 \chi(\xi) / A] \{ 1 - [A/\phi(\xi)]^{2/3} - \frac{1}{3} [\phi(\xi)]^{-2/3} \gamma^2 \} - [\lambda_0 v(\xi) / A] \ln[A/\phi(\xi)] \quad (37)$$

In the third line of (35), shear stress τ is work conjugate to γ in the energy increment per unit reference volume $\mathbf{P} : d\mathbf{F}$. Stress equilibrium (8) with (34) and (35), presuming stresses, like deformation, can only vary with the X coordinate, reduces to

$$\partial P_{xx} / \partial X = \partial P_{yx} / \partial X = \partial \tau / \partial X = 0 \quad (38)$$

Order parameter equilibrium in the first of (9) with (15) and (36) becomes

$$\begin{aligned} \xi &= -\frac{1}{2} (l/\Gamma) \phi' [\mu_0 \chi / \phi - \mu_0 \chi \phi^{-5/3} A^{2/3} - \lambda_0 (v/\phi) \ln(A/\phi)] \\ &- \frac{1}{2} (l/\Gamma) \chi' \mu_0 [\frac{3}{2} \phi^{-2/3} A^{2/3} - \frac{3}{2} - \ln(A/\phi) + \frac{1}{2} \gamma^2] - \frac{1}{4} (l/\Gamma) v' \lambda_0 [\ln(A/\phi)]^2 \end{aligned} \quad (39)$$

The same interpolation functions first introduced in (30)-(32) are invoked the remainder of this work.

First sought are spatially homogeneous solutions to (35)-(39) wherein deformation gradient and order parameter do not vary with position X :

$$A = \text{constant}, \quad \gamma = \text{constant}, \quad \xi = \text{constant} \quad (40)$$

From (35), such solutions clearly satisfy stress equilibrium (38). Also compared later is the ratio of total energy with possible transformation to elastic energy for the case when no phase transformation occurs, where for the spatially homogeneous solution,

$$\bar{\Psi} = \Psi/V = (1/V) \int_V [W(A, \gamma, \xi) + \Gamma \xi^2/l] dV = W(A, \gamma, \xi) + \Gamma \xi^2/l \quad (41)$$

$$W_0(A, \gamma) = \frac{1}{2} \mu_0 [3(A^{2/3} - 1) - 2 \ln A + \gamma^2] + \frac{1}{2} \lambda_0 (\ln A)^2$$

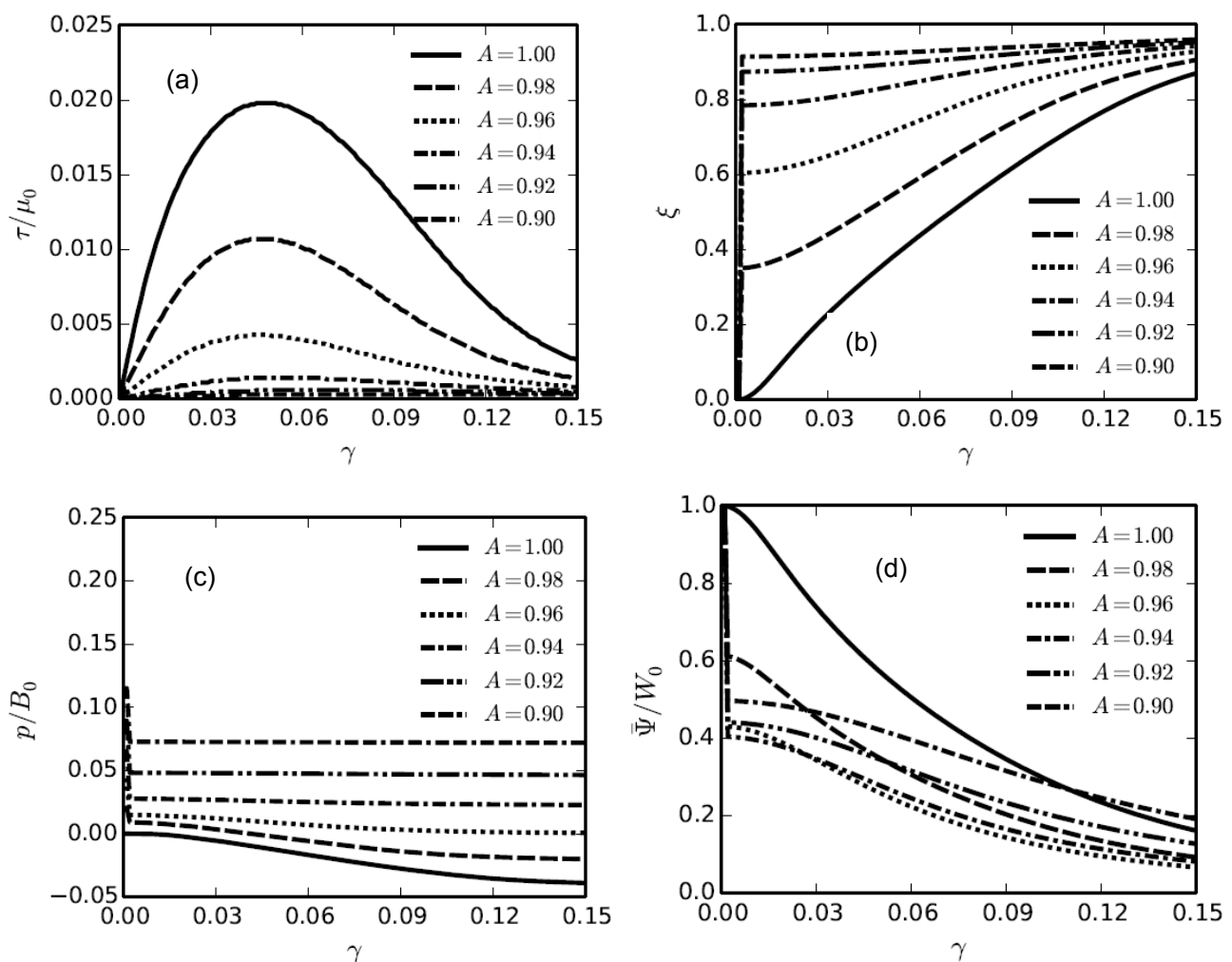


Figure 2. Shear stress (a), order parameter (b), Cauchy pressure (c), and ratio of total energy to energy for purely elastic deformation (d) for simple shear γ under spherical compression A .

Homogeneous solution data are obtained as follows for shear and compressive loading. Volume is reduced incrementally by reducing A from unity in decrements of 0.02. For each volume decrement, shear γ is increased incrementally from zero to 0.15. Equilibrium equation (39) is solved

via simple numerical iteration to obtain order parameter ξ . Once ξ is known, functions (30)-(32) are evaluated and then substituted into analytical expressions (35), (37), and (41) to determine stress components, pressure, and energies. Shown in Figure 2(a) is the shear stress τ (normalized by initial shear modulus) predicted from the phase field model at various compressive strains A . Complementary results for the order parameter and pressure (normalized by initial bulk modulus) are given in Figures 2(b) and 2(c). As volumetric compression increases (i.e., as A is reduced), pressure increases, transformation to the amorphous phase becomes more rapid, and shear strength diminishes. Complete amorphization is approached as shear strains become large, i.e., $\xi \rightarrow 1$ for $\gamma > 0.15$. Such phase field predictions agree with trends observed in DFT [11, 12] that amorphization in boron carbide is triggered by non-hydrostatic loading involving shear strain and is accelerated by increasing superposed compressive stress. As indicated by ratio values less than unity in Figure 2(d), the total energy of the phase field solution is always less than that of the purely elastic solution ($\xi = 0$) for neo-Hookean elasticity, demonstrating metastability of the latter model relative to the phase field model. Intrinsic stability at constant volumetric deformation A under dead loading by shear stress τ requires [6, 8, 16]

$$d\mathbf{P} : d\mathbf{F} = dP_{yX} dF_{yX} = d\tau d\gamma = (\partial\tau/\partial\gamma)(d\gamma)^2 > 0 \Rightarrow \partial\tau/\partial\gamma > 0 \quad (42)$$

This condition, which correlates with a positive incremental/tangent shear modulus, is first violated by each of the solutions in Figure 2(a) when shear stress τ reaches a maximum or critical value τ_C , demonstrating mechanical instability of boron carbide under simple shear loading possibly superposed on constant volumetric compression. Peak stresses at the onset of such instability are listed along with other solution variables in Table 2. As volume decreases, peak shear stress decreases, pressure increases, and the value of the order parameter at instability increases.

Table 2. Homogeneous phase field solution at critical loading or instability point.

Volume ratio A	Peak stress τ_C [GPa]	Shear γ_C	Order parameter ξ_C	Pressure p_C [GPa]
1.00	3.91	0.048	0.36	-3.02
0.98	2.11	0.047	0.53	-0.43
0.96	0.84	0.046	0.70	2.33
0.94	0.28	0.052	0.84	6.35
0.92	0.12	0.067	0.91	11.78
0.90	0.07	0.081	0.94	17.96

Now sought are spatially heterogeneous [$\xi = \xi(X)$] but stress-free solutions corresponding to vanishing of \mathbf{P} in (35) under null compression and omitting volume collapse upon transformation:

$$\begin{aligned}
 A = \Xi \rightarrow 1 &\Rightarrow \det \mathbf{F} = \phi = 1 \\
 \Rightarrow P_{xX} = P_{yY} = P_{zZ} &= 0 \\
 \tau(\gamma, \xi) = P_{xY}(\gamma, \xi) = P_{yX}(\gamma, \xi) &= \mu_0 \chi(\xi) \gamma = \mu_0 (1 - \xi)^2 \gamma = 0 \\
 \varsigma(\gamma, \xi) = \frac{1}{2} \mu_0 \chi'(\xi) \gamma^2 &= -\mu_0 (1 - \xi) \gamma^2
 \end{aligned} \quad (43)$$

The final two lines in (43) combine to imply elastic driving force in (36) must also vanish and that shear strain can be nonzero only in regions where amorphization is complete:

$$\varsigma = -\tau\gamma/(1-\xi) = 0, \quad \gamma(X) = 0 \forall \xi(X) < 1 \quad (44)$$

Order parameter equilibrium in the first of (9) becomes, for the present one-dimensional shear problem with $r = 0$ boundary conditions and full amorphization at the midpoint of the domain,

$$\partial^2 \xi / \partial X^2 - \xi / l^2 = 0, \quad (\partial \xi / \partial X)|_{X=0} = (\partial \xi / \partial X)|_{X=L} = 0, \quad \xi|_{X=L/2} = 1 \quad (45)$$

This is a homogeneous, ordinary second-order differential equation with exact solution

$$\xi(X) = \begin{cases} [e^{L/(2l)} + e^{-L/(2l)}]^{-1} (e^{X/l} + e^{-X/l}) & \text{for } X \leq L/2 \\ [e^{L/(2l)} + e^{3L/(2l)}]^{-1} e^{X/l} + [e^{-L/(2l)} + e^{-3L/(2l)}]^{-1} e^{-X/l} & \text{for } X \geq L/2 \end{cases} \quad (46)$$

Total energy per unit cross sectional area is, noting that (43) and (44) imply $W = 0$,

$$\int_0^L \Gamma [\xi^2 / l + l (\partial \xi / \partial X)^2] dX = 2\Gamma (e^{L/l} - e^{-L/l}) [e^{L/(2l)} + e^{-L/(2l)}]^{-2} \approx 2\Gamma \quad (47)$$

where the final approximation effectively becomes exact for $L > 10l$. This calculation verifies that Γ is indeed the surface energy of a localized amorphous band, the factor of two in (47) accounting for each side of the band surface. Shown in Figure 3(a) is the heterogeneous solution (46) for a domain length of $L = 25l$, verifying that the width of the localized amorphous band wherein $\xi \geq 0.75$ is approximately l . Shown in Figure 3(b) is the ratio of total energy from the homogeneous phase field solution under null volumetric compression (i.e., pure simple shear loading) to the total surface energy of the localized solution verified in (47). When this ratio in Figure 3(b) exceeds a value of unity—which occurs at $\gamma \approx 0.0125$ —the localized stress-free solution is energetically favorable to the homogeneous solution, suggesting local transformation and fracture may be expected.

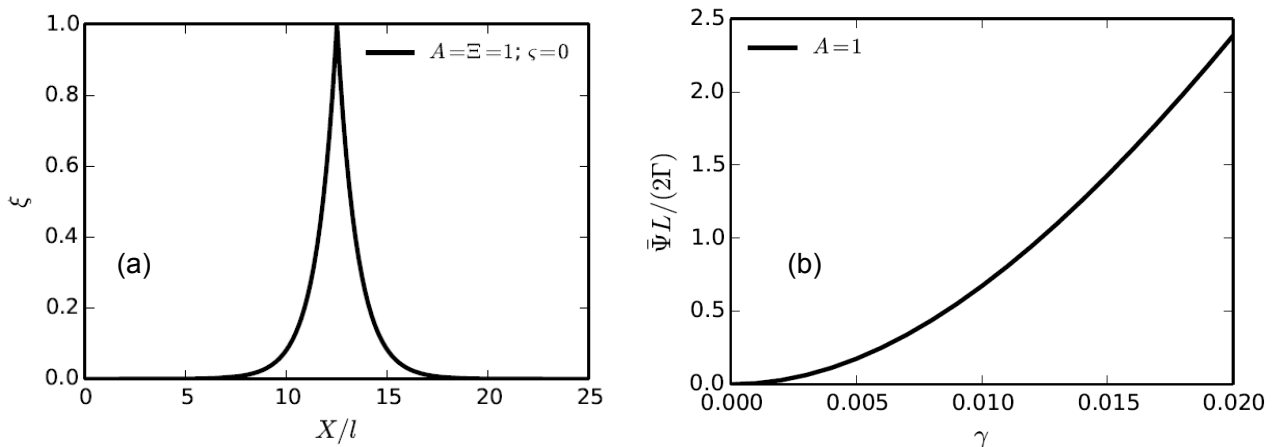


Figure 3. Order parameter profile for localized stress-free solution (a) and ratio of total energy for homogeneous phase field solution to surface energy (b) under simple shear γ .

4. Discussion

The phase field theory developed and applied in the present paper consists of the following principal components:

- Order parameter denoting transformation from crystal to amorphous/glass phase (2)

- Volumetric inelastic deformation (11) associated with mass density increase upon amorphization
- Compressible neo-Hookean nonlinear elastic strain energy (13)
- Interpolation function (30) relating order parameter increase and volume decrease (spherical eigenstrain) similar to that used to interpolate eigenshear in twinning models [19-21]
- Degraded shear modulus and fixed bulk modulus upon amorphization
- Interpolation function (31) relating order parameter increase and shear modulus decrease similar to that used to reduce elastic modulus in fracture models [22-25, 30]

The only parameters entering the phase field component of the theory are surface energy and localization width, which are obtained directly from atomic theory [9] and experiment [4, 14]. The initial bulk modulus of the neo-Hookean potential is fit to uniquely to DFT pressure-volume data [11], and the initial shear modulus is obtained directly from second-order elastic constants of DFT [10, 11]. Thus, the phase field model is considered purely predictive, with no adjustable parameters. Of course, interpolation functions such as (30)-(32) could be generalized or altered as needed in the future to match additional data for other stress-deformation states as such data become available from more extensive experimentation and atomic simulation. Furthermore, the model should be implemented in a numerical framework such as the finite element method [19-21, 25] to study boundary value problems involving more complicated geometries and boundary conditions. Extension of the theory towards a homogenized polycrystal model [16, 44] wherein multiple anisotropic B₄C crystals occupy a single material point in a computation is also foreseeable.

The present results suggest that boron carbide, under simple shear loading, should become unstable, undergo substantial amorphization, and demonstrate severe strength loss at shear strains on the order of 5%, with peak shear strengths on the order of 4 GPa, the latter value decreasing with increasing superposed pressure (Table 2). While the trends in phase field results agree with DFT predictions, maximum shear stresses observed in DFT can exceed 20 GPa, with shear strains at instability or peak load on the order of 10–15 % [11]. It is suggested that the present phase field predictions are more physically realistic when compared to real solids with defects, since it is unlikely that any brittle material could sustain such large shear stresses without undergoing mode II fracture which appears prohibited by the small system size and boundary conditions used in DFT. A complementary interpretation is that the present phase field model of shear degradation accounts for simultaneous amorphization and fracture as suggested by the form of (31), whereas prior results reported from DFT [4, 10-12] account for structure collapse but not complete bond breaking.

The present theory and solutions do not account explicitly for the presence of defects in the crystal, such as point defects, dislocations, stacking faults, and twin boundaries, all of which are known to exist in boron carbide ceramics [4, 14, 32, 33]. The model and analysis may be altered in a simple empirical way to account for defects simply by increasing or decreasing the surface energy Γ according to whether initial defect concentrations increase or decrease the energetic barrier for localization. For example, if a stacking fault promotes local amorphization, Γ may be lowered by some suitable fraction of the stacking fault energy. Alternatively, for a more realistic and predictive representation of effects of defects, the phase field theory should be extended to include additional order parameters describing (partial) dislocations and deformation twins [18-21, 45], and numerical simulations wherein initial defect geometries are resolved explicitly should be considered, as has been done elsewhere in a study of heterogeneous stress distributions in highly twinned, slip-cast boron carbide [33]. Regardless, dislocation-type defects are thought to be relatively immobile as

evidenced by the low ductility and high stiffness of boron carbide.

The model and analysis reported in this work has been limited to quasi-static loading. In impact or ballistic loading, local stress field perturbations associated with elastic wave interactions (e.g., shear and bulk compression waves) and heterogeneities (e.g., crystal defects and grain boundaries) are expected to promote amorphization. This expectation is supported by previous nonlinear analysis and simulations invoking a Born-like instability criterion for localization [16, 17], wherein dynamic deformation facilitated instability relative to static loading. The level of amorphization or structural disorder in boron carbide has also been reported as greater in dynamic indentation experiments compared to static indentation experiments [13, 46].

5. Conclusion

A nonlinear phase field theory has been developed and applied towards amorphization and shear failure in boron carbide ceramic. Analytical and iterative numerical solutions have been obtained for hydrostatic loading and for simple shear loading in conjunction with constant volumetric compression. Model predictions agree with trends reported elsewhere in experiments and quantum mechanical (DFT) simulations: transformation does not occur under purely hydrostatic loading; transformation occurs under shear loading and is promoted by superposed compressive stress; the tangent shear modulus and shear strength decrease and the material response becomes unstable upon application of sufficient shear stress or shear strain. The proposed theory, which essentially includes no adjustable or free parameters, appears to be the first phase field model of pressure-shear induced amorphization in crystalline solids.

Conflict of Interest

The authors declare there is no conflict and interest.

References

1. Gregoryanz E, Hemley R, Mao H, et al. (2000) High pressure elasticity of α -quartz: instability and ferroelastic transition. *Phys Rev Lett* 84: 3117-3120.
2. Watson G, Parker S (1995) Dynamical instabilities in α -quartz and α -berlinite: a mechanism for amorphization. *Phys Rev B* 52: 13306-13309.
3. Goel P, Mittal R, Choudhury N, et al. (2010) Lattice dynamics and Born instability in yttrium aluminum garnet, $Y_3Al_5O_{12}$. *J Phys: Condens Mat* 22: 065401.
4. Yan X, Tang Z, Zhang L, et al. (2009) Depressurization amorphization of single-crystal boron carbide. *Phys Rev Lett* 102: 075505.
5. Born M (1940) On the stability of crystal lattices I. *Math Proc Cambridge* 36: 160-172.
6. Hill R (1975) On the elasticity and stability of perfect crystals at finite strain. *Math Proc Cambridge* 77: 225-240.
7. Morris J, Krenn C (2000) The internal stability of an elastic solid. *Phil Mag A* 80: 2827-2840.
8. Clayton J, Bliss K (2014) Analysis of intrinsic stability criteria for isotropic third-order Green elastic and compressible neo-Hookean solids. *Mech Mater* 68: 104-119.

9. Fanchini G, McCauley J, Chhowalla M (2006) Behavior of disordered boron carbide under stress. *Phys Rev Lett* 97: 035502.
10. Taylor D, Wright T, McCauley J (2011) First principles calculation of stress induced amorphization in armor ceramics. *US Army Research Lab Res Rep* ARL-MR-0779, Aberdeen Proving Ground, MD.
11. Taylor D, McCauley J, Wright T (2012) The effects of stoichiometry on the mechanical properties of icosahedral boron carbide under loading. *J Phys: Condens Mat* 24: 505402.
12. Aryal S, Rulis P, Ching W (2011) Mechanism for amorphization of boron carbide B₄C under uniaxial compression. *Phys Rev B* 84: 184112.
13. Subhash G, Maiti S, Geubelle P, Ghosh D (2008) Recent advances in dynamic indentation fracture, impact damage and fragmentation of ceramics. *J Am Ceram Soc* 91: 2777-2791.
14. Chen M, McCauley J, Hemker K (2003) Shock-induced localized amorphization in boron carbide. *Science* 299: 1563-1566.
15. Grady D (2011) Adiabatic shear failure in brittle solids. *Int J Impact Eng* 38: 661-667.
16. Clayton J (2012) Towards a nonlinear elastic representation of finite compression and instability of boron carbide ceramic. *Phil Mag* 92: 2860-2893.
17. Clayton J (2013) Mesoscale modeling of dynamic compression of boron carbide polycrystals. *Mech Res Commun* 49: 57-64.
18. Koslowski M, Cuitino A, Ortiz M (2002) A phase-field theory of dislocation dynamics, strain hardening, and hysteresis in ductile single crystals. *J Mech Phys Solids* 50: 2597-2635.
19. Clayton J, Knap J (2011) A phase field model of deformation twinning: nonlinear theory and numerical simulations. *Physica D* 240: 841-858.
20. Clayton J, Knap J (2011) Phase field modeling of twinning in indentation of transparent single crystals. *Model Simul Mater Sci Eng* 19: 085005.
21. Clayton J, Knap J (2013) Phase-field analysis of fracture induced twinning in single crystals. *Acta Mater* 61: 5341-5353.
22. Kuhn C, Müller R (2012) Interpretation of parameters in phase field models for fracture. *Proc Appl Math Mec* 12: 161-162.
23. Borden M, Verhoosel C, Scott M, et al. (2012) A phase-field description of dynamic brittle fracture. *Comput Method Appl Mech Eng* 271: 77-95.
24. Voyiadjis G, Mozaffari N (2013) Nonlocal damage model using the phase field method: theory and applications. *Int J Solids Structures* 50: 3136-3151.
25. Clayton J, Knap J (2014) A geometrically nonlinear phase field theory of brittle fracture. *Int J Fracture*, submitted.
26. Clayton J (2005) Dynamic plasticity and fracture in high density polycrystals: constitutive modeling and numerical simulation. *J Mech Phys Solids* 53: 261-301.
27. Clayton J (2009) A continuum description of nonlinear elasticity, slip and twinning, with application to sapphire. *Proc R Soc Lond A* 465: 307-334.
28. Clayton J (2010) Modeling nonlinear electromechanical behavior of shocked silicon carbide *J Appl Phys* 107: 013520.
29. Clayton J (2014) Analysis of shock compression of strong single crystals with logarithmic thermoelastic-plastic theory. *Int J Eng Sci* 79: 1-20.
30. Benallal A, Marigo J (2007) Bifurcation and stability issues in gradient theories with softening. *Model Simul Mater Sci Eng* 15: S283-S295.

31. Clayton J (2011) *Nonlinear Mechanics of Crystals*, Dordrecht : Springer.
32. Ashbee K (1971) Defects in boron carbide before and after irradiation. *Acta Metall* 19: 1079-1085.
33. Sano T, Randow C (2011) The effect of twins on the mechanical behavior of boron carbide. *Metall Mater Trans A* 42: 570-574.
34. Clayton J (2012) On anholonomic deformation, geometry, and differentiation. *Math Mech Solids* 17: 702-735.
35. Clayton J (2010) Deformation, fracture, and fragmentation in brittle geologic solids. *Int J Fracture* 163: 151-172.
36. Clayton J, McDowell D, Bammann D (2006) Modeling dislocations and disclinations with finite micropolar elastoplasticity. *Int J Plasticity* 22: 210-256.
37. Clayton J (2013) Defects in nonlinear elastic crystals: differential geometry, finite kinematics, and second-order analytical solutions. *Z Angew Math Mech (ZAMM)* in press.
38. Clayton J (2014) An alternative three-term decomposition for single crystal deformation motivated by non-linear elastic dislocation solutions. *Q J Mech Appl Math* 67: 127-158.
39. Clayton J, Bammann D, McDowell D (2005) A geometric framework for the kinematics of crystals with defects. *Phil Mag* 85: 3983-4010.
40. Clayton J (2009) A non-linear model for elastic dielectric crystals with mobile vacancies. *Int J Non-Linear Mech* 44: 675-688.
41. Clayton J (2008) A model for deformation and fragmentation in crushable brittle solids. *Int J Impact Eng* 35: 269-289.
42. Ivaneshchenko V, Shevchenko V, Turchi P (2009) First principles study of the atomic and electronic structures of crystalline and amorphous B₄C. *Phys Rev B* 80: 235208.
43. Clayton J (2013) Nonlinear Eulerian thermoelasticity for anisotropic crystals. *J Mech Phys Solids* 61: 1983-2014.
44. Clayton J, McDowell D (2003) A multiscale multiplicative decomposition for elastoplasticity of polycrystals. *Int J Plasticity* 19: 1401-1444.
45. Hu S, Henager C, Chen LQ (2010) Simulations of stress-induced twinning and de-twinning: a phase field model. *Acta Mater* 58: 6554-6564.
46. Ghosh D, Subhash G, Lee C, et al. (2007) Strain-induced formation of carbon and boron clusters in boron carbide during dynamic indentation. *Appl Phys Lett* 91: 061910.

© 2014, John D. Clayton, licensee AIMS. This is an open access article distributed under the terms of the Creative Commons Attribution License (<http://creativecommons.org/licenses/by/4.0>)